# Different manifestations of triaxial shapes of the positive and negative parity bands in $^{187}$Os

S. Nandi,[1,2] G. Mukherjee ◉,[1,2,*] A. Dhal,[1,†] R. Banik ◉,[2,3] Soumik Bhattacharya,[1,2] S. Basu,[1,2] Shabir Dar ◉,[1,2]
S. Bhattacharyya,[1,2] C. Bhattacharya,[1,2] S. Kundu,[1,2] D. Paul ◉,[1,2] S. Rajbanshi,[4] S. Chatterjee,[5] S. Das,[5] S. Samanta,[5]
R. Raut,[5] S. S. Ghugre,[5] H. Pai ◉,[6] Sajad Ali,[7] S. Biswas,[8] and A. Goswami[6,‡]

[1]*Variable Energy Cyclotron Centre, Kolkata 700064, India*
[2]*Homi Bhabha National Institute, Training School Complex, Anushaktinagar, Mumbai 400094, India*
[3]*Institute of Engineering and Management, Saltlake Sector V, Kolkata 700091, India*
[4]*Department of Physics, Presidency University, Kolkata 700043, India*
[5]*UGC-DAE CSR, Kolkata Centre, Kolkata 700098, India*
[6]*Saha Institute of Nuclear Physics, Kolkata 700064, India*
[7]*Government General Degree College at Pedong, Kalimpong 734311, India*
[8]*GANIL, CEA/DSM-CNRS/IN2P3, F-14076 Caen Cedex 05, France*

The excited states of $^{187}$Os have been studied via $^{186}$W($^4$He, $3n$) $^{187}$Os reaction at a beam energy of 36 MeV. The $\gamma$ rays were detected using the Indian National Gamma Array at the Variable Energy Cyclotron Centre having seven Compton-suppressed clover high-purity germanium (HPGe) detectors and one low-energy photon spectrometer (LEPS) detector with a digital data acquisition system. The level scheme of $^{187}$Os has been extended substantially up to ≈3.86 MeV of excitation energy and $37/2\,\hbar$ of spin with the placement of more than 90 new $\gamma$ rays. All known bands have been extended and new band structures have been identified. The results show evidence of triaxial shapes for different configurations of $^{187}$Os and different manifestations of nonaxial shape have been observed in the same nucleus. A comparison of the observed band crossing frequency in $^{187}$Os with neighboring nuclei gives evidence of a deformed shell gap at $N = 110$. The experimental results are well explained using total Routhian surface calculations.

## I. INTRODUCTION

Osmium nuclei lie between the axially deformed prolate rare earth [1] and spherical Pb nuclei [2]. Many of the even-even Os isotopes are known to be $\gamma$ soft, and consequently $\gamma$ bands have been identified [3]. The neutron Fermi level in heavier Os isotopes lies in the upper half of the two high-$j$ orbitals: negative parity $\nu h_{9/2}$ and positive parity $\nu i_{13/2}$. While $\nu i_{13/2}$ is a unique positive parity orbital in this region, the other negative parity orbitals, close to the neutron Fermi level, are $p_{3/2}$ and $f_{5/2}$. Several interesting band structures would result in the odd-$A$ Os isotopes from the coupling of the odd neutron in these orbitals with the even-even core. The band structures in Os isotopes, up to neutron number $N = 109$ ($^{185}$Os) [4] are well studied but beyond that the data are very scarce, particularly for the odd-$A$ isotopes.

The observations of wobbling bands (e.g., see Ref. [5]) and $\gamma$ vibration bands (or $\gamma$ bands) are two of the interesting manifestations of the triaxial shape of a nucleus. $\gamma$ bands with one-phonon (and, only in a few cases, two-phonon) excitation(s) have been observed in different nuclei throughout the

nuclear chart [3,6–16]. The possible multiphonon deformed vibration for quadrupole shapes can have three categories with their corresponding $K$ values ($K$ is the projection of total angular momentum), $\beta\beta$ vibration ($K = 0$), $\beta\gamma$ vibration ($K = 2$), and $\gamma\gamma$ vibration ($K = 0$ and $K = 4$) [17]. In the $A \approx 180$ region, multiphonon $\gamma\gamma$ vibrational bands are reported in even-even $^{186,188}$Os nuclei [3], but have not been observed in any of the odd-$A$ isotopes in this mass region. It has been observed that the excitation energies of the $2^+$ state in a $\gamma$ band ($2_2^+$, that is the second $2^+$ state of the nucleus) in $^{184,186,188}$Os isotopes decrease with increasing mass number [3]. The decrease in excitation energy of the $2_2^+$ state suggests that the heavier Os nuclei are more $\gamma$ deformed than the lighter ones [18]. So, the heavier isotopes are ideal laboratories to study the effect of $\gamma$ deformation on the nuclear level structures. Recently, long-axis rotation, another manifestation of a triaxial nucleus, has been reported for the negative parity ($\pi h_{9/2}$) band in $^{193}$Tl ($Z = 81$) [19]. Such exotic excitations, involving the neutron $h_{9/2}$ orbital, are not observed, so far. In this context, $^{187}$Os may be an ideal nucleus to search for such long-axis rotation having an odd neutron hole in high-$j$, $h_{9/2}$ orbital.

Two negative parity bands in $^{187}$Os, based on close-lying Nilsson orbitals $1/2^-$[510] and $3/2^-$[512], were described in terms of the pseudo-Nilsson quantum numbers [20,21]. However, these bands were limited to the excitation energy

*gopal@vecc.gov.in
†Present address: ELI-NP, Mǎgurele 077126, Romania.
‡Deceased.

of 512 keV (tentative level) only. It is not known if the high level of degeneracy of a few keV, observed for the lower two excited states, continues at higher spins. In the neighboring odd-*A* isotopes, the delayed band crossing of the negative parity bands in $^{185}$Os [4] compared to that in $^{183}$Os [22] was attributed to the existence and the effect of a deformed shell gap at $N = 108$. Similar effects have been reported in the Hf and W isotopes as well [23]. However, no data exist for the band crossing frequency of any of the bands in $^{187}$Os [24].

In the present work, an experiment has been performed to study the excited states in $^{187}$Os to look for some of those phenomena which would result from the effect of one unpaired neutron, in different negative and positive parity orbitals, on the $\gamma$ deformed $^{186}$Os core [25].

## II. EXPERIMENTAL DETAILS

The excited states of $^{187}$Os were populated by the light-ion induced fusion evaporation reaction $^{186}$W($^4$He, 3$n$) $^{187}$Os at 36 MeV of beam energy, delivered from the K-130 cyclotron at the Variable Energy Cyclotron Centre, Kolkata (VECC). A stack of three $^{186}$W foils, each 300 $\mu$g/cm$^2$ thick on a 20-$\mu$g/cm$^2$ $^{12}$C backing, was used [26]. The prompt $\gamma$

rays were detected using the Indian National Gamma Array (INGA) [27]. It comprised seven Compton suppressed clover high-purity germanium (HPGe) detectors and one low-energy photon spectrometer (LEPS) detector at the time of the experiment. The clover detectors were arranged in three angles, with four at 90°, two at 125° and one at 40°, while the LEPS was kept at 40° angle. Two- and higher-fold data were recorded using a PIXIE-16 digitizer based system developed by UGC-DAE CSR Kolkata Centre [28] with the requirement of a $\gamma$-$\gamma$ coincidence master trigger. Some of the data files were recorded in singles mode for the intensity measurement of the $\gamma$ rays.

## III. DATA ANALYSIS

The raw data files were sorted and analysed using the IUCPIX [28] analysis package. The add-back data for each of the clover detectors were generated on an event-by-event basis after each crystal of the clover detectors was calibrated and gain matched. These add-back data were used to generate several $\gamma$-$\gamma$ matrices and a three-dimensional $\gamma$-$\gamma$-$\gamma$ cube for further analysis. Similarly, the data from the LEPS detector were used to generate a LEPS vs clover asymmetric matrix
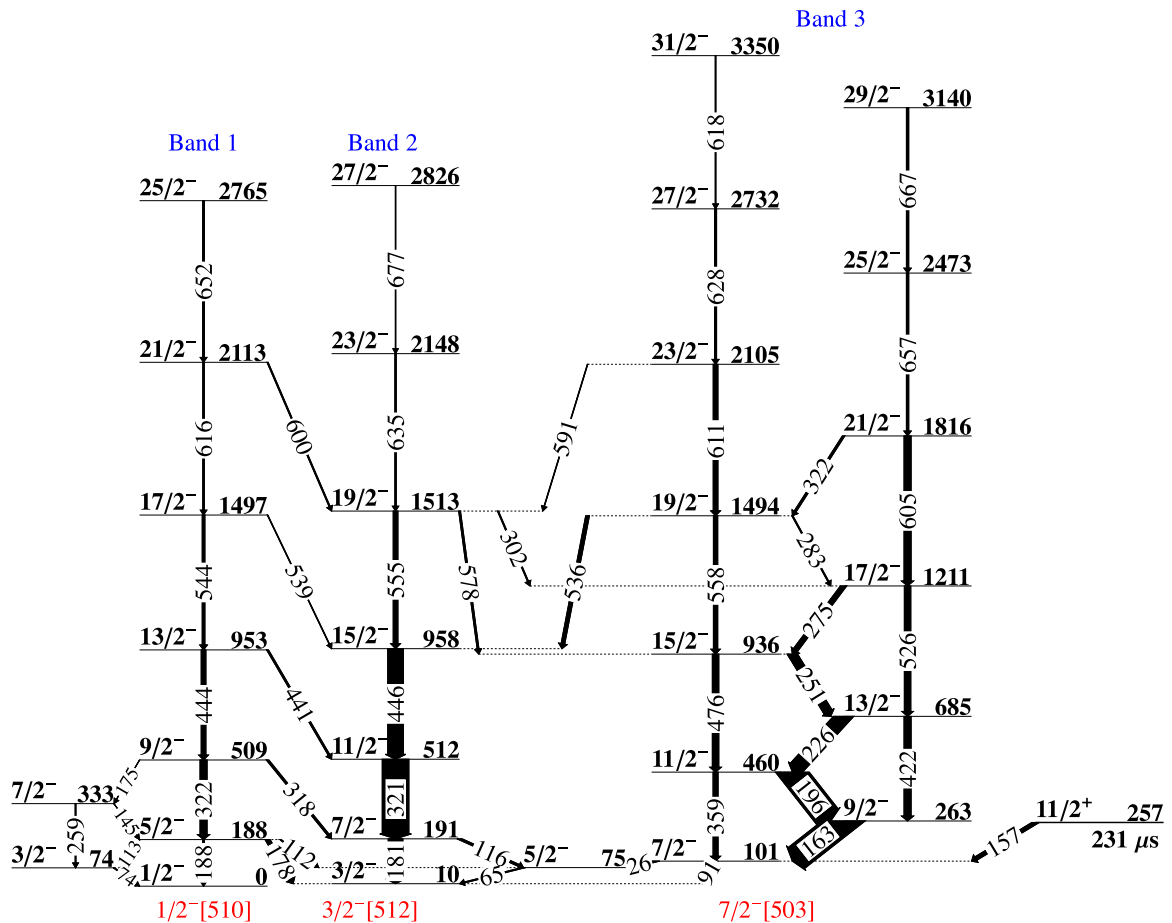


FIG. 1. Part I of the level scheme of $^{187}$Os, showing the negative parity states, from the present work. The widths of the transitions are proportional to their intensities. The level at 257 keV is a 231(2)-$\mu$s isomer. This level and its decay (157 keV) were not measured in the present experiment and are taken from Ref. [38]. The positive parity part of the level scheme, shown in Fig. 2, is built on top this isomeric state.

for further analysis. However, no add-back was done for the LEPS detector data. A total $\gamma$-$\gamma$ matrix was generated with a prompt coincidence time window of 200 ns between the add-back events of the clovers, which contained $1.4 \times 10^8$ $\gamma$-$\gamma$ coincidence events. The $\gamma$-$\gamma$ matrices and $\gamma$-$\gamma$-$\gamma$ cube were analyzed using the RADWARE [29] and INGASORT [30] analysis software packages. The level scheme of the $^{187}$Os nucleus has been constructed using the coincidence relation of the $\gamma$ rays and their intensity arguments. The spin and parity of the states were assigned from the multipolarity ($\lambda$) and the type ($E/M$) of the $\gamma$ rays decaying from the state. These two quantities ($\lambda$ and $E/M$) were determined from the measurements of the

directional correlation from oriented states (DCO) ratio [31]. In DCO ratio analysis, an asymmetric matrix was made with the data from the 125° detectors ($\theta_1$) on one axis and the 90° detectors ($\theta_2$) on the other axis. The DCO ratio ($R_{DCO}$) for $\gamma_1$, gated by another $\gamma$ ray $\gamma_2$ of known multipolarity, was obtained from the ratio of the intensities of $\gamma_1$ ($I_{\gamma_1}$) at two different angles $\theta_1$ and $\theta_2$ as

$$R_{DCO} = \frac{I_{\gamma_1}(\text{measured at } \theta_1; \text{ gated by } \gamma_2 \text{ at } \theta_2)}{I_{\gamma_1}(\text{measured at } \theta_2; \text{ gated by } \gamma_2 \text{ at } \theta_1)} \quad (1)$$

The measured $R_{DCO}$ values are close to unity for the stretched transitions with the same multipolarities of $\gamma_1$ and



FIG. 2. Part II of the level scheme of $^{187}$Os showing the positive parity states. The levels are shown above the previously known, 257-keV isomeric level. No connecting transition could be identified from band 8 to the rest of the level scheme.

TABLE I. List of $\gamma$ rays belonging to $^{187}$Os, their intensities ($I_\gamma$) relative to the intensity of the 162.4 keV $\gamma$ ray (unless mentioned otherwise), placement in the level scheme, measured values of $R_{DCO}$ and $\Delta_{PDCO}$, and the adopted multipolarities ($\lambda$). Band 5 is not included in the table as its excitation energy is not known.

| $E_\gamma$ (keV) | $E_i$ (keV) | Band no. | $I_i^\pi$ | $I_\gamma$ | $R_{DCO}$ | $\Delta_{PDCO}$ | Multipolarity |
|---|---|---|---|---|---|---|---|
| 25.9(2) | 100.5 | $3 \to 2$ | $7/2^-$ | 38(12)[a] | | | $(M1 + E2)$ |
| 65.3(2) | 74.9 | 2 | $5/2^-$ | | | | $(M1 + E2)$ |
| 74.3(2) | 74.2 | 1 | $3/2^-$ | | | | $(M1 + E2)$ |
| 86.4(2) | 1648.1 | $6 \to 5$ | $21/2^+$ | 1.2(1) | | | $(M1 + E2)$ |
| 91.1(2) | 100.5 | $3 \to 2$ | $7/2^-$ | 1.6(11)[a] | | | $(E2)$ |
| 112.4(2) | 187.5 | $1 \to 2$ | $5/2^-$ | 0.53(4) | | | $(M1 + E2)$ |
| 113.3(2) | 187.5 | 1 | $5/2^-$ | 0.39(4) | | | $(M1 + E2)$ |
| 115.8(2) | 190.7 | 2 | $7/2^-$ | 1.11(7) | 0.49(6)[b] | | $M1 + E2$ |
| 132.8(2) | 2030.7 | $7 \to 5$ | $25/2^+$ | 0.21(2) | | | $(M1 + E2)$ |
| 145.3(2) | 333.2 | 1 | $7/2^-$ | 0.06(1) | | | $(M1 + E2)$ |
| 162.4(2) | 419.4 | 4 | $13/2^+$ | 100 | 0.41(1)[c] | | $M1 + E2$ |
| 162.9(2) | 263.4 | 3 | $9/2^-$ | 13.6(8) | 0.62(3)[d] | $-0.06(4)$ | $M1 + E2$ |
| 175.4(2) | 508.9 | 1 | $9/2^-$ | 0.08(1) | | | $(M1 + E2)$ |
| 177.8(2) | 187.5 | $1 \to 2$ | $5/2^-$ | 2.29(13) | 0.76(4)[e] | | $M1 + E2$ |
| 178.5(2) | 1826.9 | 4 | $25/2^+$ | 1.09(7) | 0.44(6)[c] | | $M1 + E2$ |
| 179.9(2) | 1562.2 | $5 \to 6$ | $21/2^+$ | 0.96(8) | | | $(M1 + E2)$ |
| 181.0(2) | 190.7 | 2 | $7/2^-$ | 7.5(4) | 0.93(3)[b] | 0.13(10) | $E2$ |
| 187.7(2) | 187.5 | 1 | $5/2^-$ | 0.88(5) | 0.99(7)[e] | | $E2$ |
| 196.4(2) | 459.8 | 3 | $11/2^-$ | 13.6(8) | 0.58(3)[f] | $-0.07(5)$ | $M1 + E2$ |
| 199.1(2) | 618.3 | 4 | $15/2^+$ | 37.6(9) | 0.49(1)[g] | | $M1 + E2$ |
| 200.8(2) | 818.7 | 4 | $17/2^+$ | 21.9(7) | 0.68(2)[h] | | $M1 + E2$ |
| 203.0(2) | 1287.8 | 4 | $21/2^+$ | 4.11(16) | 0.47(5)[c] | $-0.25(16)$ | $M1 + E2$ |
| 214.1(2) | 1341.4 | 5 | $19/2^+$ | 4.23(14) | 0.61(7)[i] | $-0.13(11)$ | $M1 + E2$ |
| 220.9(2) | 1562.2 | 5 | $21/2^+$ | 15.9(5) | 0.73(4)[i] | $-0.06(4)$ | $M1 + E2$ |
| 225.6(2) | 685.4 | 3 | $13/2^-$ | 7.7(4) | 0.48(2)[j] | $-0.14(9)$ | $M1 + E2$ |
| 232.7(2) | 1127.4 | 5 | $17/2^+$ | 5.8(2) | 0.59(3)[k] | $-0.15(10)$ | $M1 + E2$ |
| 246.4(2) | 2203.1 | $5 \to 6$ | $25/2^+$ | 2.6(1) | 0.72(8)[l] | | $M1 + E2$ |
| 250.6(2) | 936.0 | 3 | $15/2^-$ | 4.6(2) | 0.52(3)[d] | $-0.11(8)$ | $M1 + E2$ |
| 253.9(2) | 2284.6 | 7 | $27/2^{(+)}$ | 1.71(8) | 0.84(11)[m] | | $M1 + E2$ |
| 254.8(2) | 1382.5 | $6 \to 5$ | $19/2^+$ | 3.7(2) | 0.54(5)[n] | $-0.14(10)$ | $M1 + E2$ |
| 259.1(2) | 333.2 | 1 | $7/2^-$ | 0.42(4) | | | $(E2)$ |
| 265.9(2) | 1648.1 | 6 | $21/2^+$ | 1.29(7) | 0.67(11)[n] | $-0.07(5)$ | $M1 + E2$ |
| 266.3(2) | 1085.0 | 4 | $19/2^+$ | 13.2(5) | 0.48(1)[c] | $-0.11(6)$ | $M1 + E2$ |
| 275.2(2) | 1211.2 | 3 | $17/2^-$ | 2.6(2) | 0.59(4)[f] | $-0.06(2)$ | $M1 + E2$ |
| 282.6(2) | 1493.8 | 3 | $19/2^-$ | 0.54(4) | 0.60(6)[f] | | $M1 + (E2)$ |
| 296.3(2) | 2327.0 | 7 | $29/2^+$ | 7.6(5) | 0.90(10)[n] | 0.24(13) | $E2$ |
| 301.8(2) | 2628.8 | 7 | $33/2^+$ | 4.0(4) | 0.95(5)[m] | 0.17(10) | $E2$ |
| 302.2(2) | 1513.4 | $2 \to 3$ | $19/2^-$ | 0.53(4) | 0.62(9)[f] | | $M1 + E2$ |
| 305.3(2) | 2203.1 | 5 | $25/2^+$ | 6.01(19) | 0.75(10)[c] | $-0.18(10)$ | $M1 + E2$ |
| 308.5(2) | 1956.5 | 6 | $23/2^+$ | 1.06(5) | 0.69(10)[n] | | $M1 + E2$ |
| 318.1(2) | 508.9 | $1 \to 2$ | $9/2^-$ | 1.05(14) | 0.67(7)[o] | $-0.17(14)$ | $M1 + E2$ |
| 320.8(2) | 1833.5 | | $21/2^+$ | 0.90(14) | | | $(M1 + E2)$ |
| 321.1(2) | 2949.9 | 7 | $37/2^+$ | 3.5(4) | 1.00(9)[m] | 0.23(11) | $E2$ |
| 321.3(2) | 511.9 | 2 | $11/2^-$ | 13.6(11) | 0.95(2)[b] | 0.13(5) | $E2$ |
| 321.6(2) | 508.9 | 1 | $9/2^-$ | 3.6(3) | 1.01(3)[p] | 0.17(11) | $E2$ |
| 321.9(2) | 1815.7 | 3 | $21/2^-$ | 1.1(2) | 0.53(7)[f] | | $M1 + E2$ |
| 335.7(2) | 1898.1 | 5 | $23/2^+$ | 18.3(8) | 0.66(5)[c] | $-0.14(10)$ | $M1 + E2$ |
| 345.4(2) | 2243.5 | $\to 5$ | $25/2^+$ | 1.27(5) | 0.51(7)[k] | $-0.17(11)$ | $M1 + E2$ |
| 353.6(2) | 3328.0 | 5 | $31/2^+$ | 3.70(14) | 0.67(11)[k] | $-0.23(11)$ | $M1 + E2$ |
| 359.3(2) | 459.8 | 3 | $11/2^-$ | 2.56(9) | 1.03(7)[f] | 0.11(8) | $E2$ |
| 360.9(2) | 1648.6 | 4 | $23/2^+$ | 4.74(19) | 0.52(4)[c] | $-0.13(8)$ | $M1 + E2$ |
| 361.0(2) | 618.3 | 4 | $15/2^+$ | 21.3(5) | 0.88(6)[h] | 0.09(8) | $E2$ |
| 363.8(2) | 2974.3 | 5 | $29/2^+$ | 3.9(2) | 0.52(6)[k] | $-0.14(9)$ | $M1 + E2$ |
| 371.3(2) | 2204.8 | | $(23/2^+)$ | 0.80(5) | | | $(M1 + E2)$ |
| 376.9(2) | 2275.4 | $\to 5$ | $27/2^+$ | 1.88(9) | 0.91(12)[k] | 0.15(12) | $E2$ |

TABLE I. (*Continued.*)

| $E_\gamma$ (keV) | $E_i$ (keV) | Band no. | $I_i^\pi$ | $I_\gamma$ | $R_{DCO}$ | $\Delta_{PDCO}$ | Multipolarity |
|---|---|---|---|---|---|---|---|
| 381.8(2) | 2657.0 | | $(31/2^+)$ | 0.55(3) | | | $(E2)$ |
| 385.4(2) | 1512.7 | →5 | $19/2^+$ | 2.5(2) | 0.50(4)[n] | −0.20(9) | $M1 + E2$ |
| 399.0(2) | 818.7 | 4 | $17/2^+$ | 27.7(11) | 0.99(4)[h] | 0.22(5) | $E2$ |
| 407.3(2) | 2610.4 | 5 | $27/2^+$ | 11.6(5) | 0.65(9)[k] | −0.09(7) | $M1 + E2$ |
| 421.9(2) | 685.4 | 3 | $13/2^-$ | 3.6(2) | 0.92(5)[j] | 0.09(8) | $E2$ |
| 434.9(2) | 1562.2 | 5 | $21/2^+$ | 14.5(5) | 0.93(6)[i] | 0.26(9) | $E2$ |
| 440.3(2) | 2643.4 | →5 | $27/2^+$ | 5.1(2) | 0.63(6)[k] | −0.17(10) | $M1 + E2$ |
| 440.8(2) | 952.6 | 1 → 2 | $13/2^-$ | 0.87(6) | 0.69(2)[q] | −0.15(12) | $M1 + E2$ |
| 443.5(2) | 952.6 | 1 | $13/2^-$ | 2.4(2) | 0.93(9)[p] | 0.18(14) | $E2$ |
| 445.8(2) | 957.8 | 2 | $15/2^-$ | 8.0(4) | 1.07(4)[q] | 0.10(5) | $E2$ |
| 446.5(2) | 1341.4 | 5 | $19/2^+$ | 5.5(3) | 0.83(9)[m] | 0.15(9) | $E2$ |
| 451.0(2) | 1833.5 | →6 | $21/2^+$ | 2.17(9) | 0.54(15)[n] | −0.14(11) | $M1 + E2$ |
| 466.4(2) | 1085.0 | 4 | $19/2^+$ | 18.9(9) | 1.0(2)[h] | 0.12(7) | $E2$ |
| 468.2(2) | 2030.7 | 7 → 5 | $25/2^+$ | 11.8(7) | 1.01(11)[g] | 0.13(11) | $E2$ |
| 468.9(2) | 1287.8 | 4 | $21/2^+$ | 29.0(13) | 1.00(4)[c] | 0.09(3) | $E2$ |
| 475.7(2) | 894.7 | 5 → 4 | $15/2^+$ | 9.8(5) | 0.53(5)[k] | −0.09(6) | $M1 + E2$ |
| 476.3(2) | 936.0 | 3 | $15/2^-$ | 3.3(3) | 1.03(7)[r] | 0.09(4) | $E2$ |
| 476.9(2) | 1562.2 | 5 → 4 | $21/2^+$ | 5.5(8) | 0.62(6)[c] | −0.16(11) | $M1 + E2$ |
| 488.0(2) | 1382.5 | 6 → 5 | $19/2^+$ | 3.4(2) | 1.03(10)[l] | 0.24(12) | $E2$ |
| 508.9(2) | 1127.4 | 5 → 4 | $17/2^+$ | 13.7(10) | 0.58(2)[k] | −0.11(7) | $M1 + E2$ |
| 520.6(2) | 1648.1 | 6 → 5 | $21/2^+$ | 3.8(2) | 0.98(8)[n] | 0.22(12) | $E2$ |
| 523.0(2) | 1341.4 | 5 → 4 | $19/2^+$ | 2.6(2) | 0.62(11)[i] | −0.14(12) | $M1 + E2$ |
| 525.8(2) | 1211.2 | 3 | $17/2^-$ | 3.3(6) | 1.07(5)[d] | 0.12(7) | $E2$ |
| 536.1(2) | 1493.8 | 3 → 2 | $19/2^-$ | 1.9(1) | 1.04(9)[r] | 0.17(13) | $E2$ |
| 538.7(2) | 3182.1 | | $29/2^{(+)}$ | 0.65(4) | 0.62(8)[k] | | $M1 + E2$ |
| 539.0(2) | 1826.9 | 4 | $25/2^+$ | 10.8(4) | 1.00(4)[c] | 0.11(4) | $E2$ |
| 539.4(2) | 1497.0 | 1 → 2 | $17/2^-$ | 0.28(2) | 0.70(10)[b] | −0.11(5) | $M1 + E2$ |
| 544.4(2) | 1497.0 | 1 | $17/2^-$ | 1.36(6) | 1.04(12)[p] | 0.17(13) | $E2$ |
| 553.1(2) | 2837.7 | 7 | $31/2^{(+)}$ | 1.15(8) | 0.91(10)[m] | | $E2$ |
| 554.3(2) | 2203.1 | 5 → 4 | $25/2^+$ | 17.0(2) | 0.79(5)[c] | −0.19(11) | $M1 + E2$ |
| 555.4(2) | 1513.4 | 2 | $19/2^-$ | 2.4(2) | 0.99(7)[q] | 0.14(8) | $E2$ |
| 557.7(2) | 1493.8 | 3 | $19/2^-$ | 2.2(1) | 0.98(10)[d] | 0.12(7) | $E2$ |
| 562.2(2) | 3399.9 | 7 | $(35/2^+)$ | 0.44(6) | | | $(E2)$ |
| 563.5(2) | 1648.6 | 4 | $23/2^+$ | 23.1(7) | 0.92(2)[g] | 0.08(4) | $E2$ |
| 563.7(2) | 1382.5 | 6 → 4 | $19/2^+$ | 9.7(4) | 0.42(3)[l] | −0.12(8) | $M1 + E2$ |
| 573.9(2) | 1956.5 | 6 | $23/2^+$ | 3.0(2) | 1.02(11)[c] | 0.22(13) | $E2$ |
| 577.7(2) | 1513.4 | 2 → 3 | $19/2^-$ | 0.93(6) | 1.04(14)[f] | 0.13(11) | $E2$ |
| 590.6(2) | 3201.0 | | $31/2^+$ | 1.49(6) | 1.08(15)[k] | 0.19(8) | $E2$ |
| 591.3(2) | 2104.5 | 3 → 2 | $23/2^-$ | 0.26(3) | | | $(E2)$ |
| 599.5(2) | 2113.0 | 1 → 2 | $21/2^-$ | 0.55(5) | 0.57(13)[b] | | $M1 + E2$ |
| 604.5(2) | 1815.7 | 3 | $21/2^-$ | 3.6(2) | 1.02(7)[d] | 0.09(6) | $E2$ |
| 610.5(2) | 2104.5 | 3 | $23/2^-$ | 2.4(2) | 1.00(10)[d] | 0.16(11) | $E2$ |
| 612.0(2) | 1898.1 | 5 → 4 | $23/2^+$ | 0.19(2) | | | $(M1 + E2)$ |
| 616.0(2) | 2113.0 | 1 | $21/2^-$ | <0.78 | 1.10(13)[e] | | $E2$ |
| 617.6(2) | 2444.5 | 4 | $29/2^+$ | 12.0(5) | 1.05(8)[c] | 0.19(5) | $E2$ |
| 618.0(2) | 3350.4 | 3 | $31/2^-$ | 0.35(4) | 1.02(12)[s] | 0.11(10) | $E2$ |
| 624.5(2) | 2137.3 | | $23/2^{(+)}$ | 1.30(5) | 0.96(15)[n] | | $E2$ |
| 627.6(2) | 2275.4 | | $27/2^+$ | 0.27(2) | | | $(M1 + E2)$ |
| 627.9(2) | 2732.4 | 3 | $27/2^-$ | 1.03(6) | 1.03(16)[f] | 0.22(12) | $E2$ |
| 635.0(2) | 2148.4 | 2 | $23/2^-$ | 0.70(4) | 1.04(10)[f] | 0.14(12) | $E2$ |
| 637.7(2) | 894.7 | 5 → 4 | $15/2^+$ | 8.5(4) | 0.93(6)[k] | 0.22(10) | $E2$ |
| 652.0(2) | 2765.0 | 1 | $25/2^-$ | <0.91 | 1.02(13)[e] | | $E2$ |
| 654.6(2) | 2303.2 | 4 | $27/2^+$ | 6.0(2) | 0.95(5)[g] | 0.15(6) | $E2$ |
| 657.1(2) | 2472.8 | 3 | $25/2^-$ | 1.20(5) | 0.98(4)[d] | 0.19(13) | $E2$ |
| 667.1(2) | 3139.9 | 3 | $29/2^-$ | 1.18(5) | 0.91(14)[j] | 0.19(16) | $E2$ |
| 668.7(2) | 1956.5 | 6 → 4 | $23/2^+$ | 2.14(7) | 0.69(11)[n] | | $M1 + E2$ |
| 677.2(2) | 2825.6 | 2 | $27/2^-$ | 0.22(2) | 1.07(21)[f] | | $E2$ |
| 686.6(2) | 3131.1 | 4 | $33/2^+$ | 3.7(2) | 1.00(11)[c] | 0.19(9) | $E2$ |

TABLE I. (*Continued.*)

| $E_\gamma$ (keV) | $E_i$ (keV) | Band no. | $I_i^\pi$ | $I_\gamma$ | $R_{DCO}$ | $\Delta_{PDCO}$ | Multipolarity |
|---|---|---|---|---|---|---|---|
| 708.0(2) | 1127.4 | 5 → 4 | $17/2^+$ | 7.1(3) | 0.91(4)[k] | 0.18(10) | $E2$ |
| 717.8(2) | 3328.0 | 5 | $31/2^+$ | 0.82(4) | 0.92(19)[k] | | $E2$ |
| 722.9(2) | 1341.4 | 5 → 4 | $19/2^+$ | 3.55(13) | 0.94(11)[i] | 0.24(9) | $E2$ |
| 725.1(2) | 3856.2 | 4 | $37/2^+$ | 0.58(4) | 1.10(14)[c] | | $E2$ |
| 732.2(2) | 3035.4 | 4 | $31/2^+$ | 1.5(1) | 1.02(17)[g] | 0.29(17) | $E2$ |
| 743.8(2) | 1562.2 | 5 → 4 | $21/2^+$ | 1.4(2) | 1.04(14)[c] | | $E2$ |
| 783.3(2) | 3818.7 | 4 | $35/2^+$ | 0.50(6) | 0.90(16)[g] | | $E2$ |
| 922.0(2) | 1341.4 | 5 → 4 | $19/2^+$ | 7.2(3) | 0.99(7)[m] | −0.05(3) | $M3 + E4$ |

[a]From LEPS data, not normalized to clovers; [b]From the 446-keV ($E2$) gate; [c]From the 399-keV ($E2$) gate; [d]From the 422-keV ($E2$) gate; [e]From the 322-keV ($E2$) gate; [f]From the 476-keV ($E2$) gate; [g]From the 466-keV ($E2$) gate; [h]From the 539-keV ($E2$) gate; [i]From the 361-keV ($E2$) gate; [j]From the 526-keV ($E2$) gate; [k]From the 435-keV ($E2$) gate; [l]From the 574-keV ($E2$) gate; [m]From the 468-keV ($E2$) gate; [n]From the 708-keV ($E2$) gate; [o]From the 444-keV ($E2$) gate; [p]From the 188-keV ($E2$) gate; [q]From the 181-keV ($E2$) gate; [r]From the 610-keV ($E2$) gate; [s]From the 628-keV ($E2$) gate.

$\gamma_2$. Otherwise, the values are ≈0.6 for a dipole transition gated by a stretched quadrupole transition. The value of $R_{DCO}$ also depends on the initial spin alignment of the excited nuclei, which was denoted by the width of the substate population $\sigma/I$ and also on the mixing ratio ($\delta$) of the $\gamma$ transition. In most cases of heavy-ion-induced fusion evaporation reactions the value of $\sigma/I$ is taken as ≈0.3. But, in an $\alpha$-induced fusion evaporation reaction, we observed earlier that the width of the substate population $\sigma/I$ is wider, with a value of ≈0.37 [32].

In order to determine the type ($E/M$) of the $\gamma$ rays to assign the parity of the states, polarization asymmetry measurements were performed. Data from the detectors at 90° were used to measure the polarization asymmetry [33]. The polarization asymmetry ($\Delta_{PDCO}$) is defined as

$$\Delta_{PDCO} = \frac{a(E_\gamma)N_\perp - N_\parallel}{a(E_\gamma)N_\perp + N_\parallel}, \quad (2)$$

where $N_\perp$ and $N_\parallel$ are the Compton scattered events in the planes perpendicular and parallel to the reaction plane, respectively, inside a clover detector. To measure $N_\perp$ and $N_\parallel$, two asymmetric matrices of $N_\perp$ vs all detectors and $N_\parallel$ vs all detectors were generated. The asymmetric response of the clover segments was corrected by the factor $a(E_\gamma)$ $(=\frac{N_\parallel}{N_\perp})$, which was determined using an unpolarized radioactive source. This gives the value $a = 1.042(10)$, which is comparable to the value determined in Ref. [34] for the same setup. The positive and negative values of the polarization asymmetry $\Delta_{PDCO}$ imply whether the $\gamma$ ray is of electric ($E$) or magnetic ($M$) type, respectively.

## IV. EXPERIMENTAL RESULTS

The level scheme of $^{187}$Os is shown in two parts: the negative parity part is shown in Fig. 1 and the positive parity part is shown in Fig. 2. The experimental $\gamma$-ray transition energies ($E_\gamma$), the level energies ($E_i$), the spins and parities of the initial ($I_i^\pi$) levels, the $R_{DCO}$ and $\Delta_{PDCO}$ values, along with the adopted multipolarities of the $\gamma$ rays are tabulated in Table I. The level scheme of $^{187}$Os has been significantly extended in the present work.

### A. Negative parity bands

#### 1. Band 1 and band 2

The spin and parity of the bandheads of bands 1 and 2 were assigned as $1/2^-$ and $3/2^-$ and were known up to the level energy at 509 and 512 keV, respectively, from the previous work of Sodan *et al.* [24]. However, the levels at 509 and 512 keV and a low-lying level at 341 keV were tentatively placed in the level scheme in Ref. [24]. In the present work, bands 1 and 2 have been extended up to the excitation energies of 2765 and 2826 keV and angular momenta of $25/2\,\hbar$ and $27/2\,\hbar$, respectively. All the $\gamma$ rays of band 1 and band 2 including the newly observed ones are shown in the double gated spectra of Fig. 3. The double gate on the $\gamma$ rays of band 2 established the newly observed transitions of band 2 and also the connections between bands 3 and 2 as shown in Fig. 3. The energy levels of bands 1 and 2 are very close to each other, with a separation of only a few keV. In the present analysis, the closely spaced tentative levels of 512 and 509 keV could be separated. In Fig. 4 the spectra with a single gate on 536 and 544 keV
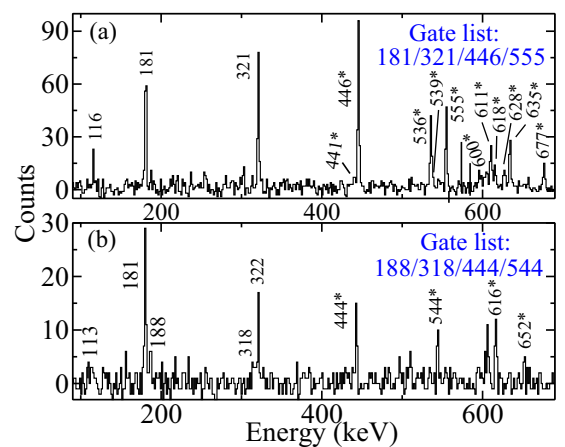


FIG. 3. Sum double-gated spectra from gate lists (a) 181, 321, 446, 555 keV and (b) 188, 318, 444, 544 keV transitions in bands 2 and 1, respectively. Newly observed transitions are marked by asterisks (∗).
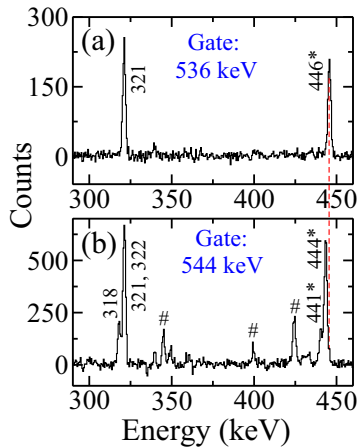
FIG. 4. Coincidence spectra gated by (a) 536 keV and (b) 544 keV showing the close-lying $\gamma$ rays of bands 2 and 1. The new $\gamma$ rays are marked by asterisks (∗) and the contaminant peaks are marked by #.

are shown. The 444- and 446-keV lines, which decay to 509- and 512-keV levels, are clearly seen as separate $\gamma$ rays. The 441-keV line is also seen in the 544-keV gate but not in the 536-keV gate. Both 321- and 322-keV lines are seen in these two gated spectra, but the 318-keV line is seen only in the 544-keV gate. This again confirms the two separate levels at 509 and 512 keV. Similarly, the other closely spaced levels could be separated out by appropriate gating transitions. However, it can be seen from Fig. 1 that the separation energies between the levels of bands 1 and 2 increase with spin.

### 2. Band 3

The low-lying states in band 3 were known from earlier works and the $7/2^-[503]$ configuration of the $7/2^-$ band head at 101 keV was proposed by Malmskog *et al.* [35]. This configuration was adopted in later works as well [24,36]. The decay transitions from this level, however, could not be observed in all earlier works as they are of low energies and highly converted (large electron conversion coefficient, $\alpha_T$) transitions of energies 26 and 91 keV. A good estimate of their total intensity, $\gamma$-ray intensity, and $\alpha_T$ was given by Harmatz *et al.* [37]. It was reported that the total transition intensity of 91 keV is about two orders of magnitude less than the 26-keV one [37]. In the present work, the low-energy, 26-keV $\gamma$ ray could be observed in the LEPS detector, as shown in Fig. 5. This spectrum is a projection from the LEPS vs clover matrix with sum gates (put on the clovers) on the strong transitions in band 3. The 91-keV line is also seen, albeit with very low counts, in this spectrum. The $\gamma$-ray branching ratio of the 26-keV, $M1$ and the 91-keV, $E2$ transitions has been obtained as 96 : 4 in the present work, which is in good agreement with the values reported by Harmatz *et al.* (94.5 : 5.5) and the value (95.5 : 4.5) quoted in Ref. [38].

Band 3 of bandhead spin and parity $7/2^-$ was reported tentatively up to 1211 keV with a tentatively placed $\gamma$ ray of energy 526 keV, decaying from that level [24]. In the present work, band 3 has been extended up to the excitation energy
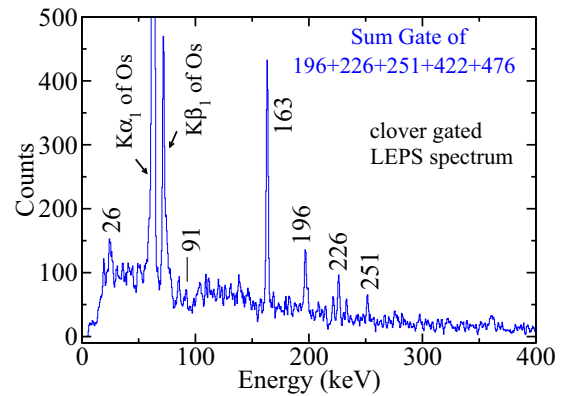


FIG. 5. Clover gated LEPS spectrum projected from the clover vs LEPS $\gamma$-$\gamma$ matrix. Projection of the sum gate of 196, 226, 251, 422, and 476 keV in the LEPS detector shows the low-energy, 26-keV transition.

of 3350 keV and $31/2\,\hbar$ angular momentum. The tentatively placed $\gamma$ ray of energy 526 keV has been confirmed in the double-gated spectra of 163, 196, 226, and 251 keV as shown in Fig. 6. All the new transitions of band 3 and the connecting transitions between bands 2 and 3, shown in Fig. 6, are marked by asterisks (∗).

### B. Positive parity bands

#### 1. Band 4

The single-gated spectrum with a gate on the earlier-known, 162-keV transition shows most of the $\gamma$ rays placed in band 4 and the new $\gamma$ rays belonging to bands 5 and band 6, as shown in Fig. 7. Band 4, based on the $\nu i_{13/2}$ configuration with bandhead spin and parity of $11/2^+$, was known up to the excitation energy of $\approx$1.1 MeV [24]. In the present experiment, band 4 has been extended up to the excitation energy of 3856 keV. All the new $\gamma$ rays of band 4 have been confirmed in the sum double-gated spectra shown in Fig. 8
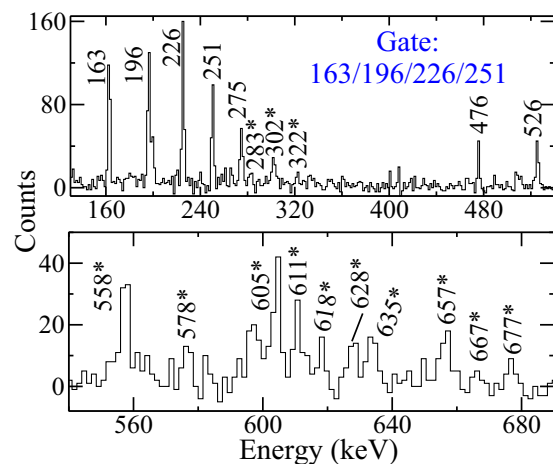


FIG. 6. Sum double-gated spectra corresponding to gate list 163, 196, 226, 251 keV of band 3 projected from $\gamma$-$\gamma$-$\gamma$ cube. New $\gamma$ rays are marked by asterisks (∗).
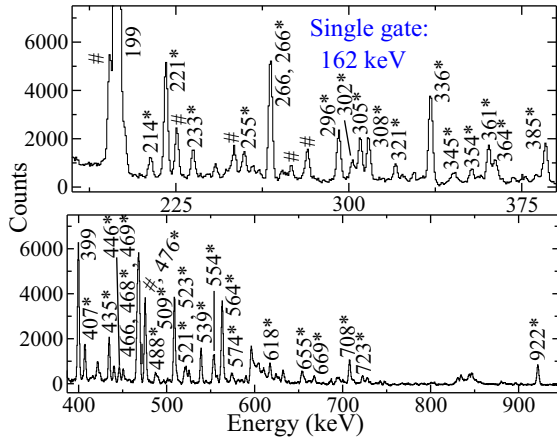
FIG. 7. Single-gated (162 keV of band 4) spectrum projected from the $\gamma$-$\gamma$ matrix. New $\gamma$ rays are marked by asterisks (∗) and the contaminant ones are marked by #.

with gates put on a few low-lying $\gamma'$s in the two signature partners.

### 2. Band 5 and band 6

Band 5 and band 6 have been identified for the first time in this work. Several connecting transitions have been observed between bands 5 and 4 as well as between bands 6 and 5. The representative double-gated spectrum in Fig. 9 and the single-gated spectrum in Fig. 10 show some of these new connecting as well as the in-band transitions along with the known $\gamma$ rays.

### 3. Band 7 and band 8

The transitions in band 7 can be seen in the double-gated spectra presented in Fig. 11. The known $\gamma$ rays are also seen in this spectrum. The $\gamma$ rays in band 8 have been observed to be in coincidence with each other as shown in a representative single-gated spectrum in Fig. 12, but no known transition of
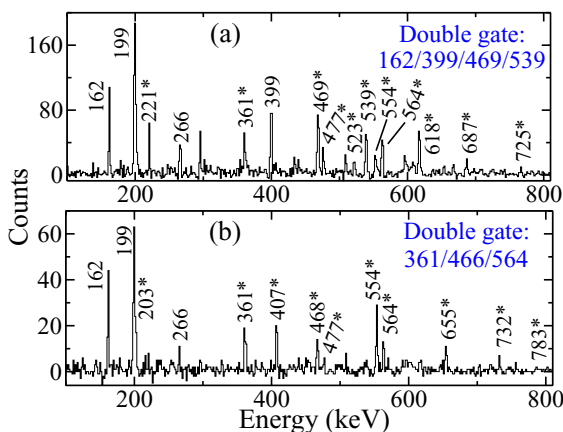


FIG. 8. Sum double gated spectra corresponding to (a) gate list 162, 399, 469, 539 keV and (b) gate list 361, 466, 564 keV of band 4 projected from the $\gamma$-$\gamma$-$\gamma$ cube. New $\gamma$ rays are marked by asterisks (∗).



FIG. 9. Double gated spectrum with gates on 162 keV in band 4 and 221 keV in band 5 showing the $\gamma$ rays in the newly observed band 5 and the connecting transitions. New $\gamma$ rays are marked by asterisks (∗).

$^{187}$Os could be found in coincidence with this band. However, we strongly believe that this band structure belongs to $^{187}$Os as this set of coincident $\gamma$ rays could not be identified in any of the neighboring nuclei which might be populated in the present reaction. In a light-ion, like $\alpha$, induced reaction, the number of produced nuclei are very limited and the energy was chosen so as to maximize the production of $^{187}$Os. Therefore, these strong $\gamma$ rays should belong to $^{187}$Os and the excitation energy of this band is expected to be low so that this band decays by a very low-energy and/or highly converted transition which could not be detected in the present experiment.

### 4. 922 keV, M3 + E4 transition

A 922-keV transition has been placed in the positive parity part of the level scheme, decaying from the 1341-keV, $19/2^+$ state in band B5 to the 419-keV, $13/2^+$ state in band B4. This $\gamma$ ray can be clearly seen in the single- and double-gated spectra of Figs. 7 and 9, respectively. The spins and parities of the initial and the final states of this transition, which were
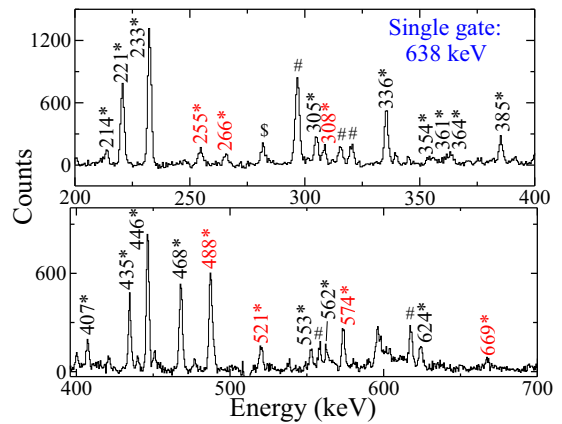


FIG. 10. Spectra gated by 638 keV, which is a connecting $\gamma$ ray from band 5 to band 4. The intra- and interband transitions in and from band 6 are shown in red color. New $\gamma$ rays are marked by asterisks (∗) and the known contaminants from $^{186}$Os and the ones which could not be placed in the level scheme are marked by # and $.
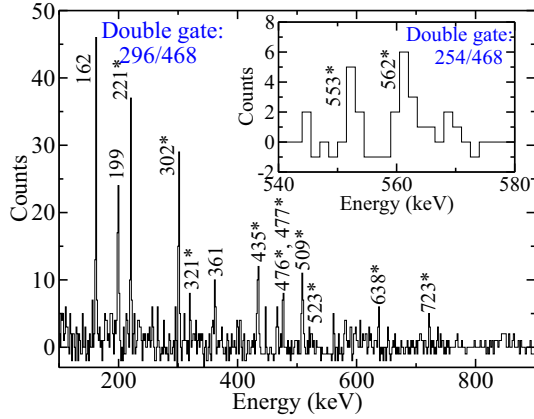
FIG. 11. Double gated spectra showing the $\gamma$ rays in band 7 along with some of the known transitions in $^{187}$Os. New $\gamma$ rays are marked by asterisks ($*$).

determined from the other $\gamma$ rays decaying from these states, suggest $M3 + E4$ multipolarity for the 922-keV $\gamma$. The DCO ratio of this transition has been measured as 0.99(7) when gated by an $E2$ $\gamma$ ray (see Table I). This is consistent with the calculated value for a $M3/E4$ mixing ratio of $\delta_{M3/E4} \approx -0.5$. The low negative value of the measured $\Delta_{PDCO}$ also supports the $M3 + E4$ assignment of the 922-keV transition.

It may be noted that there are total 5 $\gamma$ rays which decay out from the 1341-keV state. These are 214.2 keV ($M1 + E2$), 446.5 keV ($E2$), 523.0 keV ($M1 + E2$), 722.9 keV ($E2$), and 922.0 keV ($M3 + E4$). The half-life of this state can be estimated from the partial half-lives of these individual decays calculated by considering their single-particle (s.p) estimates and measured branching ratios. The estimated half-life of this state lies between 0.6 ps and 0.2 ns (the two values are obtained considering $M$ and $E$ types for the mixed transitions, respectively). Therefore, the observation of the decay of this state in our prompt measurement is also consistent.

## V. DISCUSSION

### A. Negative parity bands

In $^{187}$Os, the $3p_{3/2}$ and $2f_{5/2}$ negative parity neutron single-particle orbitals lie close to the Fermi level for neutron
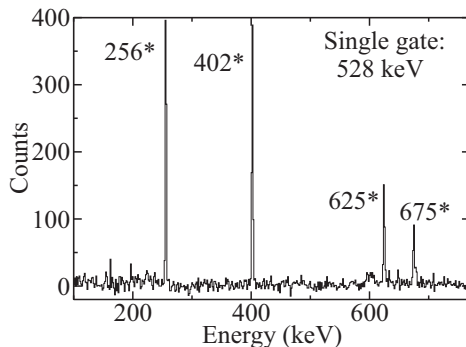


FIG. 12. Spectrum with single gate of 528-keV $\gamma$ ray showing the transitions in band 8. New $\gamma$ rays are marked by asterisks ($*$).

number $N = 111$. The high-$\Omega$ Nilsson orbitals $9/2^-$[505] and $7/2^-$[503] are also accessible near the neutron Fermi level of $^{187}$Os at low ($\beta_2 \approx 0.15$) and moderate ($\beta_2 \approx 0.3$) deformations, respectively. Therefore, various rotational bands in $^{187}$Os may be understood from the coupling of the odd neutron in these orbitals with the even-even core of $^{186}$Os [25]. The rotational bands 1 and 2 in $^{187}$Os are known to have the Nilsson configurations $1/2^-$[510] and $3/2^-$[512] while band 3 is known to be based on the $7/2^-$[503] Nilsson configuration. The $7/2^-$ state of the later configuration is an isomer in the odd-$A$ Os isotopes [36].

The nearly degenerate bands 1 and 2, which were known only up to $11/2^-$ [24], have been investigated in the framework of pseudospin symmetry by various authors [20,21]. In the present work, these bands have been extended up to $27/2^-$.

The concept of pseudospin symmetry was known for several years after the works of Arima [39] and Hecht [40]. Certain Nilsson orbitals with $\Delta\Omega = 1$ and $\Delta\Lambda = 2$ are nearly degenerate and remain parallel as a function of deformation ($\beta_2$) [41,42]. Two such orbitals with Nilsson quantum numbers $\Omega[Nn_z\Lambda - 2]$ and $\acute{\Omega}[Nn_z\Lambda]$ can be transformed in to pseudo-Nilsson quantum numbers of $\tilde{\Omega}[\tilde{N}\tilde{n}_z\tilde{\Lambda}]$, where $\Omega = (\Lambda - 2) + 1/2$ and $\acute{\Omega} = \Lambda - 1/2$. The pseudo-Nilsson quantum numbers can be written as $\tilde{N} = N - 1$, $\tilde{\Lambda} = \Lambda - 1$, and $\tilde{\Omega} = \Omega$. In this framework, the two pseudospin orbitals obey the relation $\tilde{\Omega} = (\tilde{\Lambda} \pm 1/2)$, similar to the orbital splitting due to spin-orbit interaction. Therefore, two nearly degenerate or closely spaced bands will be experimentally observed with similar properties and the amount of degeneracy between the bands depends on the strength of the pseudo-spin-orbit interaction. Also, the difference of the aligned angular momenta between the bands will be $1\hbar$ [43], coming from the difference of the $\tilde{\Omega}$ ($\tilde{\Lambda} + 1/2$ and $\tilde{\Lambda} - 1/2$) values of the two bands.

Bands 1 and 2 in $^{187}$Os, having Nilsson quantum numbers of 1/2[510] and 3/2[512] with natural parity, can be transformed to the pseudo-Nilsson quantum numbers 1/2, 3/2[$\tilde{4}\tilde{1}\tilde{1}$], and these two bands have been identified as pseudospin partner bands [20]. The amount of degeneracy between these pseudospin partner bands is observed to be very small, within a few keV. Similarly, the bands based on these two configurations in $^{185}$Os and $^{189}$Os were also identified as pseudospin partner bands [20,44]. The amount of degeneracy between the pseudospin partner bands in the three Os isotopes is shown in Fig. 13. It can be seen that the degeneracy is within a few keV in case of $^{187,189}$Os but, it is large and increases rapidly with spin for $^{185}$Os. In case of $^{187}$Os, the energy difference starts to increase above $17/2\hbar$ of spin.

The aligned angular momenta, $i_x$, as a function of rotational frequency, $\omega$, for the twin bands in $^{187}$Os have been plotted and compared with those in $^{185,189}$Os in Fig. 14. The data for the later two isotopes were taken from Ref. [44]. The Harris reference parameters $j_0 = 20\ \hbar^2\ \text{MeV}^{-1}$ and $j_1 = 94\ \hbar^4\ \text{MeV}^{-3}$ were used. The differences in $i_x$ ($\Delta i_x$) between the twin bands in these isotopes are also shown in the inset. It can be seen that $\Delta i_x$ remains close to $1\hbar$ in $^{187}$Os, which
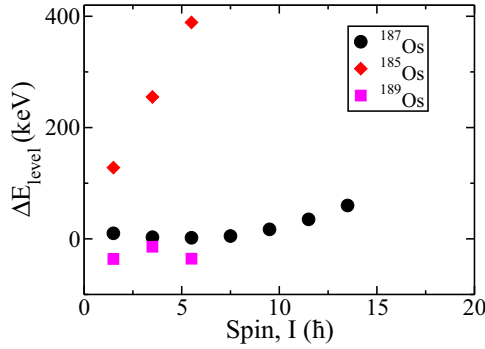
FIG. 13. The energy separation between the pseudospin partner bands $[\Delta E_{level} = E(I)_{3/2[512]} - E(I-1)_{1/2[510]}]$ as a function of spin $(I)$ in $^{185}$Os, $^{187}$Os, and $^{189}$Os. Data on $^{185}$Os are from Ref. [44] and those on $^{189}$Os are from Refs. [20,45]. For $^{185}$Os, higher spin members, for which the differences increase further, are not shown

is similar to that observed in the other two isotopes and also to the pseudo-Nilsson doublets in other nuclei [46,47]. In the case of $^{187}$Os, the difference remains almost constant at $1\hbar$ up to about $\hbar\omega \approx 0.2$ MeV and starts to deviate only near the band crossing frequency.

In the present work, as both bands 1 and 2 in $^{187}$Os have been extended, the band crossing of these bands can be clearly observed, and can be compared with that in $^{185}$Os as shown in Fig. 14. It can be seen that the band crossings are taking place at nearly the same frequency ($\hbar\omega \approx 0.3$ MeV) for bands 1 and 2 in $^{187}$Os. These band crossing frequencies are also similar to those in $^{185}$Os (in $^{189}$Os, the data are limited to below the band crossing). It is, therefore, suggested that the configurations of these bands in the two isotopes and the origin of their band crossings are of similar nature. If the band crossings in these isotopes are due to the neutron pair alignment, they may take place in either the $h_{9/2}$ or $i_{13/2}$ orbital with a total gain in alignment of $\approx 8\hbar$ or $\approx 12\hbar$, respectively. Similarly, in the case of a proton pair alignment, it would be either in the high-$j$, $h_{11/2}$ orbital or low-$j$ positive-parity orbitals. For $h_{11/2}$, the gain in alignment would be $\approx 10\hbar$. The existing data on $^{185}$Os and the present data on $^{187}$Os indicate a large gain due to
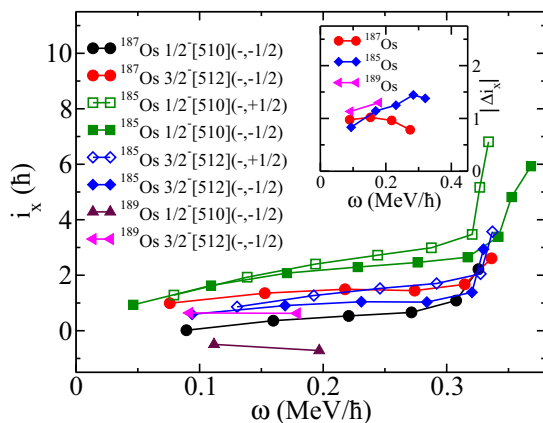


FIG. 14. Aligned angular momentum $i_x$ as a function of rotational frequency ($\omega$) for the twin bands 1 and 2 in $^{185,187}$Os.
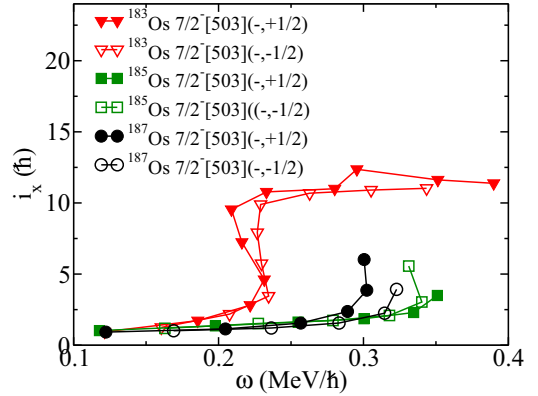


FIG. 15. Aligned angular momentum $i_x$ as a function of rotational frequency ($\omega$) for the $\nu 7/2^-$[503] band in $^{183,185,187}$Os.

alignment, but the data are not enough to observe the complete gain. Therefore, although it seems that the alignments for both $^{185,187}$Os take place in the high-$j$ orbitals, more high-spin data are required to get the exact nature of their alignments.

Band 3, based on the $\nu h_{9/2}$ configuration, has also been extended in the present work up to a spin such that the band crossing due to the first pair alignment can be seen in this band. Rotational bands, similar to band 3, are also known in the neighboring lighter odd-$A$ isotopes of Os, and have the Nilsson configuration of $7/2^-$[503]. The aligned angular momentum ($i_x$) as a function of rotational frequency ($\omega$) of the bands based on this configuration has been plotted for $^{183}$Os ($N = 107$) [22], $^{185}$Os ($N = 109$) [4], and $^{187}$Os ($N = 111$) nuclei in Fig. 15. A delayed band crossing, due to the alignment of a pair of neutrons, was earlier known in $^{185}$Os at the crossing frequency of $\hbar\omega_c \approx 0.34$ MeV [4] as compared to $\hbar\omega_c \approx 0.23$ MeV for $^{183}$Os. This delayed crossing in $^{185}$Os was explained from the existence of a deformed shell gap at $N = 108$. The crossing frequency for $^{187}$Os has been observed to be $\hbar\omega_c \approx 0.31$ MeV in the present work. This high value of $\hbar\omega_c$ in $^{187}$Os compared to that in $^{183}$Os, and close to that in $^{185}$Os, indicates the presence of another deformed shell closure at $N = 110$ but perhaps with a slightly less pronounced gap than that at $N = 108$.

It is worth noting that such delayed crossings with even higher crossing frequency of $\hbar\omega_c \approx 0.4$ MeV have been reported in the isotopes of W ($Z = 74$) and Hf ($Z = 72$) nuclei with neutron numbers $N = 108$ and $N = 110$ [23]. It was pointed out by Ngijoi-Yogo *et al.* that the smaller values of the crossing frequencies in Os isotopes compared to the axially symmetric Hf and W isotopes may be due to the presence of $\gamma$ deformation in Os nuclei [23].

The energy staggering of a rotational band, defined as $S(I) = E(I) - [E(I+1) + E(I-1)]/2$, also provides useful nuclear structure information. $S(I)$ as a function of spin $(I)$ has been plotted in Fig. 16 for the $7/2^-$[503] bands in different odd-$A$ Os and W isotopes. All the isotopes show very similar behavior of $S(I)$ with no staggering at lower spins. However, at higher spins, they differ for the Os isotopes. $^{183}$Os ($N = 107$) and $^{187}$Os ($N = 111$) have similar (large) staggering above $I = 9.5\hbar$. In the case of $^{185}$Os ($N = 109$), the staggering is small and in opposite phase to that of $^{183,187}$Os.
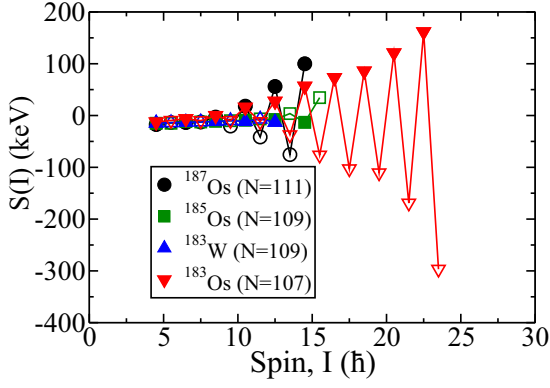
FIG. 16. Energy staggering [$S(I)$] vs spin ($I$) for the $\nu 7/2^-$[503] band in $^{183,185,187}$Os and $^{183}$W.



FIG. 17. Quadrupole moments vs rotational frequency ($\omega$) for the $\nu 7/2^-$[503] band in $^{187}$Os. Experimental values are compared with the results obtained from the TRS calculations.

Data on W isotopes, corresponding to the same neutron numbers, are not known at higher spins for comparison. The large signature splitting of band 3 in $^{187}$Os, which is based on a high-$\Omega$ configuration ($\Omega = 7/2$) suggests the presence of triaxial deformation.

In the case of a triaxial nucleus with no symmetry axis, rotation is possible around any of the three axes of the nucleus. However, the most favored rotation is the rotation around the medium axis, which needs the least energy to excite rotational motion as the moment of inertia is the maximum around the medium axis for a triaxial nucleus [48]. Rotation around the unfavored long axis has been identified recently in a few nuclei in the $A \approx 190$ and other lighter mass regions [19,49]. In the Lund convention, rotation around the long axis corresponds to deformation parameter $\gamma \approx -90°$ [48]. Such nonaxial shapes with $\gamma \approx -90°$ have been predicted by the cranked-Nilsson-Strutinski calculations for $^{193}$Tl and $^{191}$Au nuclei with neutron number $N = 112$ [19,50]. One of the ways to test the long-axis rotation is to identify if the nucleus possesses a shape with $\gamma \approx -90°$. This can be done by comparing the measured quadrupole moment with that determined from the calculated deformation parameters ($\beta_2$ and $\gamma$). Quadrupole moment can be experimentally obtained from the lifetimes of the states in the rotational band. However, in the present work, the lifetimes of the states could not be measured. So, the quadrupole moments of the states in band 3 have been estimated in the following way. The intensity ratios between the $\Delta I = 1$ and $\Delta I = 2$ transitions can be used to obtain the $B(M1)/B(E2)$ transition strength ratio [51]. The $B(M1)$ and $B(E2)$ values can be calculated by the well-known equations

$$B(M1) = \frac{3}{4\pi}\mu_N^2(g_K - g_R)^2 K^2 \frac{(I-K)(I+K)}{I(2I+1)}, \quad (3)$$

$$B(E2) = \frac{5}{16\pi}Q_\circ^2 \frac{3(I-K)(I-K-1)(I+K)(I+K-1)}{(2I-2)(2I-1)I(2I+1)}, \quad (4)$$

where $g_k$ and $g_R$ ($\approx \frac{Z}{A}$) are the $g$ factors, $I$ is the initial spin of the branching state, $K$ is the bandhead spin, and $Q_\circ$ is the quadrupole moment. In this estimation the $g_k$ value of 0.15 is taken, corresponding to the neutron in $\nu h_{9/2}$ from Ref. [52].
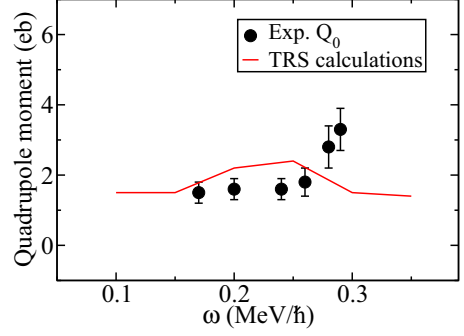
The experimental [$B(M1)/B(E2)$] values are then compared with these calculated [$B(M1)/B(E2)$] values to determine the quadrupole moments for the states in band 3. The quadrupole moments $Q_\circ$, thus obtained, for $11/2^-$ to $21/2^-$ states in band 3 have been plotted in Fig. 17.

In order to relate the above quadrupole moments with the shape of $^{187}$Os, total Routhian surface (TRS) calculations were performed, as described in the following section, for the configuration corresponding to band 3 in $^{187}$Os at several rotational frequencies ($\hbar\omega$). Two of the TRS plots in the ($\beta_2$-$\gamma$) plane are shown in Fig. 18 for two rotational frequencies. It can be seen that the minima in the TRSs are obtained at $\beta_2 \approx 0.18$ and $\gamma \approx -90°$. The value of the triaxial parameter $\gamma$ remains within $\gamma = -95°$ to $-85°$ for all the values of $\hbar\omega$. Therefore, the TRS calculations clearly suggest a stable triaxial deformation for $^{187}$Os with $\gamma$ deformation that will favor the long-axis rotation.

From the $\beta_2$ and $\gamma$ values corresponding to the minimum of the TRS calculations for each value of $\hbar\omega$, the quadrupole moment can be calculated using the equation [17]

$$Q_0 = \frac{3ZA^{2/3}r_\circ^2}{\sqrt{5\pi}}\beta_2(1 + 0.16\beta_2)\frac{\cos(\gamma + 30°)}{\cos 30°}. \quad (5)$$

These theoretical values of quadrupole moments are also shown in Fig. 17. A good agreement of experimental values and the theoretical ones supports the presence of stable long axis rotation in $^{187}$Os.
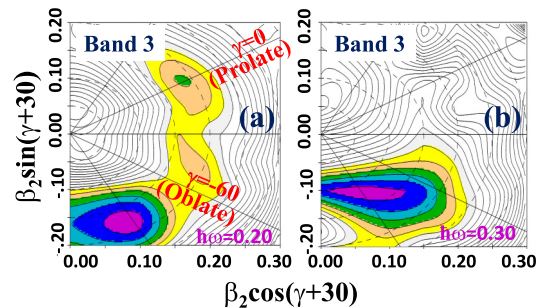


FIG. 18. TRS plots for the configuration corresponding to band 3 in $^{187}$Os at $\hbar\omega$ 0.20 MeV (a) and 0.30 MeV (b). The contours are 250 keV apart.
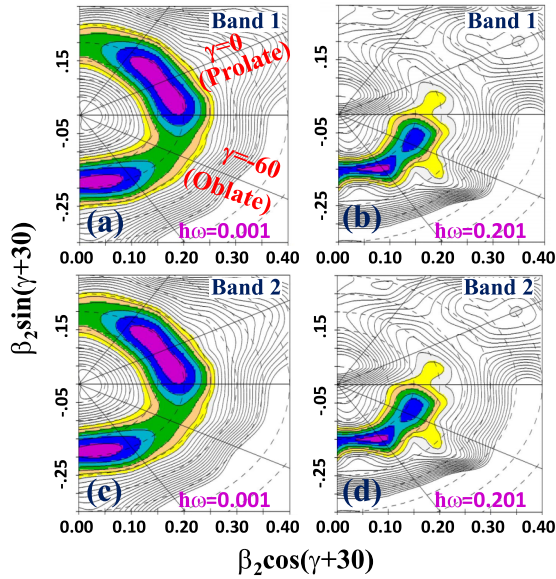
FIG. 19. TRS plots for the configuration corresponding to band 1 [(a) and (b)] and band 2 [(c) and (d)] in $^{187}$Os at $\hbar\omega$ 0.001 and 0.201 MeV. The contours are 250 keV apart.

### *1. TRS calculations*

The total Routhian surface (TRS) calculations were performed in the Nilsson-Strutinsky formalism with Woods-Saxon potential to calculate the single-particle energies [53,54]. The detailed technical procedure is given in Ref. [55]. The total Routhian energies were calculated in the ($\beta_2$, $\gamma$, $\beta_4$) mesh points for different values of rotational frequency $\hbar\omega$. The calculated energies are plotted for each $\hbar\omega$ as contour plots in the $\beta_2$-$\gamma$ plane after minimization on $\beta_4$. In the Lund convention, $\gamma = 0°$ corresponds to prolate and $\gamma = -60°$ corresponds to oblate shapes. The deformation of a nucleus for a particular configuration at a particular $\hbar\omega$ corresponds to the minimum in the contour plots of the potential energies.

The TRS calculations, performed for the configurations corresponding to band 1 and band 2 in $^{187}$Os, are shown in Fig. 19 for the two values of $\hbar\omega$. It can be seen from these figures that the surfaces look very similar for the twin bands. This is consistent with the observed degeneracy between the two bands in terms of their level energies. The surfaces for both the bands show $\gamma$ softness at the lower values of rotational frequencies, that is near the band heads with a mean at about prolate shape ($\gamma \approx 0°$). At higher frequency, the calculations predict moderate triaxiality with $\gamma \approx -90°$. It may be noted that the structure of $^{187}$Os in these low-$\Omega$ configurations of the twin bands are very similar to band 3 with high-$\Omega$ configuration. This is a possible reason for the strong connections observed at higher spins from band 3 to bands 1 and 2.

### B. Positive parity bands

Band 4 in $^{187}$Os, with two signature partners, is similar to the 11/2$^+$[615] band observed in its neighboring odd-*A* isotope $^{185}$Os [4]. The aligned angular momenta ($i_x$) of both the signature partners of this band in these two nuclei are
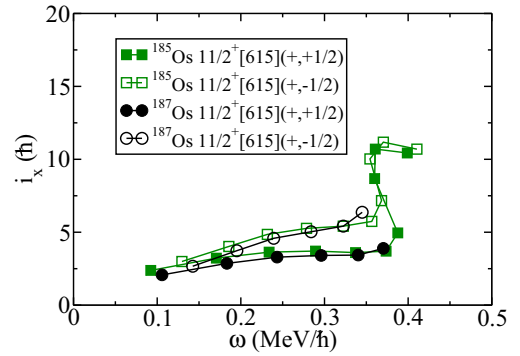


FIG. 20. Aligned angular momentum $i_x$ as a function of rotational frequency ($\omega$) for the $\nu 11/2^+$[615] band in $^{185,187}$Os.

plotted as a function of rotational frequency ($\omega$) in Fig. 20. The similar nature of $i_x$ suggests similar configuration of this band in the two isotopes. The sudden increase in $i_x$ above $\omega \approx 0.4$ MeV/$\hbar$ in $^{185}$Os suggests that the band crossing, due to the alignment of a pair of particles, has taken place at that rotational frequency [4]. In $^{187}$Os, the new data are not enough to observe the band crossing but they clearly show that the band crossing does not take place in this $N = 111$ isotope at a smaller frequency than that in the $N = 109$ isotope $^{185}$Os. There is, however, indication that the pair alignment in $^{187}$Os takes place at a similar frequency as that in $^{185}$Os. This suggests similar shape and similar origin of their band crossings.

The energy staggering $S(I)$ of band 4 has been plotted in Fig. 21 as a function of spin and compared with the neighboring odd-*A* isotope $^{185}$Os. Large energy staggering is observed for both isotopes. Such a large staggering for a band based on a high-$\Omega$ orbital suggests triaxial shape in these nuclei. In the case of triaxiality, since $\Omega$ is not a good quantum number, the low-$\Omega$ components mix with the high-$\Omega$ ones in the wave function to produce large staggering. The $K$ mixing due to the $\gamma$ softness has been discussed in regard to the transitions observed between states with large $\Delta K$ in $^{185}$Os [4].

As mentioned before, there are several interconnecting transitions from the newly observed band 5 to band 4 and also from band 6 to band 5. Such level structures and transitions
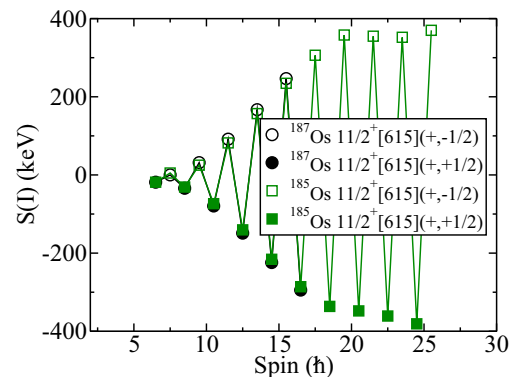


FIG. 21. Energy staggering $S(I)$ vs spin ($\hbar$) for the $\nu 11/2^+$[615] band in $^{185,187}$Os.
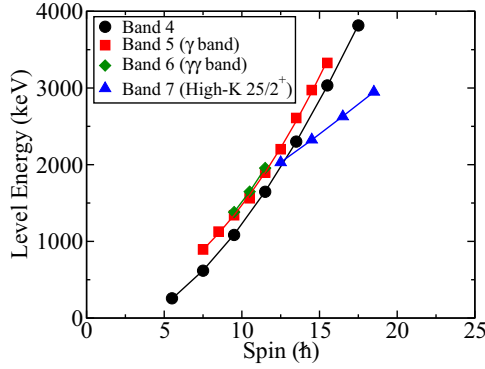
FIG. 22. Plot of level energy (in KeV) vs spin (in $\hbar$) of bands 4, 5, 6, and 7 in $^{187}$Os.



FIG. 23. Total aligned angular momentum ($I_X$) vs rotational frequency ($\omega$) for bands 4, 5, and 6.

are indicative of one- and two-phonon $\gamma$-vibrational bands, as reported in other nuclei [15,16]. These are also similar to the $\gamma$-vibrational bands observed in the neighbouring odd-$A$ nucleus $^{185}$Os [4] and in the even-even neighboring isotopes $^{186,188}$Os [3,25,56]. Therefore, band 5 and band 6, which are $\Delta I = 1$ bands, may be considered as the $\gamma$ and $\gamma\gamma$ vibrational bands in $^{187}$Os. The origin of the lowest-lying, i.e., $15/2^+$ and $19/2^+$, states in these bands, can be considered as due to the coupling of the $11/2^+[615]$ neutron with the $K_{1\gamma} = 2^+$ and $K_{2\gamma} = 4^+$ states of the $\gamma$ and $\gamma\gamma$ vibrational bands in $^{186}$Os. Other higher-spin states in these bands have been generated in the similar way by the coupling of the odd neutron with the $\Delta I = 1$, $\gamma$ band and $\gamma\gamma$ band in the $^{186}$Os even-even core.

In order to check the similarities of the structures between bands 4, 5 and 6, the level energy vs angular momentum of these three bands are plotted (Fig. 22) and fitted using the rotational energy formula

$$E(I, K) = E_K + A[I(I + 1) - K^2].\tag{6}$$

The values of the inertia parameter $A$ for these bands have been determined from the fit as 12.41, 12.82, and 13.05 MeV/$\hbar^2$ for bands 4, 5, and 6, respectively. Similar values of the inertia parameters indicate similar structures for these bands.

Figure 23 shows plots of the projection of the total angular momentum along the rotational axis ($I_x$) as a function of rotational frequency ($\omega$) for the three bands 4, 5, and 6. The slope of the curve in this plot gives the moment of inertia. It can be seen from this figure that the slope of the one-phonon $\gamma$ band is very similar to the main band (band 1). Since there is only one data point possible for the two-phonon $\gamma\gamma$ band, the slope cannot be determined for this band, but the data point for this band matches well with the other bands. The similarities in $I_x$ and, thereby, the moment of inertia in these bands is consistent with the expectation of a $\gamma$ vibrational band.

The bandhead excitation energies of the $\gamma$ and $\gamma\gamma$ bands in $^{187}$Os have been compared with those in the neighboring even-even isotopes $^{186,188}$Os in Table. II. It shows that the bandhead excitation energy of the $\gamma$ band in $^{188}$Os is lower than that in $^{186}$Os and the one in $^{187}$Os, observed in this work, nicely follows the systematics. The decrease of the bandhead excitation energy indicates that the heavier Os isotopes are
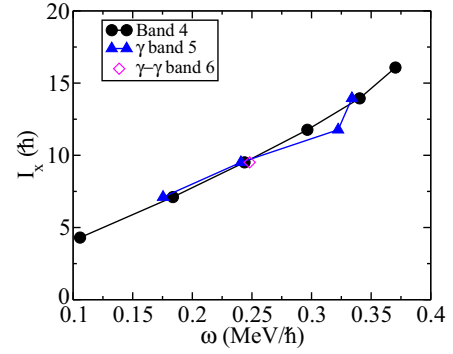
more $\gamma$ deformed than the lighter ones. In the case of $\gamma\gamma$ bands, the excitation energy ($E_{2\gamma}$) for the odd-$A$, $^{187}$Os isotope is the lowest. Ideally, the ratio of $E_{2\gamma}$ and $E_{1\gamma}$ should be close to 2, which is the case for $^{188}$Os. In the cases of $^{186}$Os and $^{187}$Os, the ratios are very similar but slightly less than the ideal value. This suggests that the $\gamma\gamma$ vibrational bands in these isotopes may not be pure.

The $\gamma$ band of a nucleus results from its nonaxial shape, due to either a rigid triaxial shape or a $\gamma$-soft (or $\gamma$-unstable) shape. Empirically, these can be distinguished from the double energy differences of the levels of the $\gamma$ band, $E_S(I)$, involving three consecutive levels of spins $I$, $I - 1$, and $I - 2$. This has been defined by Casten as [17]

$$E_S(I) = \Delta E_I - \Delta E_{I-1},\tag{7}$$

where $\Delta E_I = E_I - E_{I-1}$ and $\Delta E_{I-1} = E_{I-1} - E_{I-2}$. The values of $E_S(I)$ for an even-even nucleus will be lower for the odd-spin states in the case of $\gamma$-rigid shape while it will be lower for the even-spin states for $\gamma$-soft deformation, and accordingly they obey the Davydov model or Wilets-Jean model, respectively [17]. The values of $E_S(I)$ are shown in Fig. 24 as a function of spin for the $\gamma$ bands in the even-even core $^{186}$Os and in $^{187}$Os. It can be seen that the phases of the variation of $E_S(I)$ with spin are opposite in the two cases; while it corresponds to a $\gamma$-soft shape for $^{186}$Os, a $\gamma$-rigid shape is apparent for $^{187}$Os.

In case of the $\gamma$-rigid shape, the nonaxial deformation parameter $\gamma$ can be extracted from the Davydov model [18] using the energy ratio $E_{2_2^+}/E_{2_1^+}$ of the first two $2^+$ states for even-even nuclei [17]. In a similar way, in case of the odd-$A$ nucleus $^{187}$Os, the deformation parameter $\gamma$ can be extracted using the energy ratio $E_{15/2_2^+}/E_{15/2_1^+}$ of the first two $15/2^+$ states with respect to the bandhead excitation energy of the

TABLE II. The bandhead excitation energies of $\gamma$ and $\gamma\gamma$ bands in $^{186,187,188}$Os. Data for the even-even isotopes are from Ref. [3,25].

| Nucleus | $K_{1\gamma}$ | $E_{1\gamma}$ (keV) | $K_{2\gamma}$ (keV) | $E_{2\gamma}$ | $E_{2\gamma}/E_{1\gamma}$ |
|---|---|---|---|---|---|
| $^{186}$Os | $2^+$ | 768 | $4^+$ | 1353 | 1.76 |
| $^{187}$Os | $15/2^+$ | 637 | $19/2^+$ | 1125 | 1.77 |
| $^{188}$Os | $2^+$ | 633 | $4^+$ | 1280 | 2.02 |
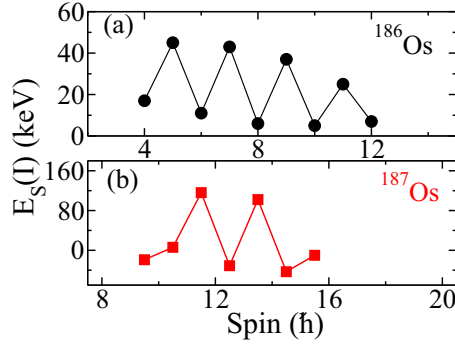
FIG. 24. Plot of double energy differences $E_S(I)$ as a function of spin for the $\gamma$ bands in $^{186}$Os (a) and $^{187}$Os (b). Data for $^{186}$Os are from Ref. [3].

positive parity main band, using the equation [17]

$$\frac{E_{15/2_2^+}}{E_{15/2_1^+}} = \frac{1+X}{1-X}, \tag{8}$$

where

$$X = \sqrt{1 - \frac{8}{9}\sin^2(3\gamma)}. \tag{9}$$

In this equation, $\gamma$ is the nonaxial deformation parameter. The deduced $\gamma$ value for the $\gamma$ band in $^{187}$Os is $|\gamma| \approx 30°$, which is the largest triaxiality in a nucleus.

Band 8 in Fig. 2 has also been observed for the first time in $^{187}$Os in this work. In the neighboring lighter odd-$A$ Os isotopes, the $9/2^+[624]$ band has been reported in $^{181}$Os [57], $^{183}$Os [22], and $^{185}$Os [4] at lower excitation energies. Therefore, this band 8 can be assigned the same configuration. The aligned angular momentum ($i_x$) as a function of rotational frequency ($\omega$) of this band has been plotted and compared with the bands based on the $9/2^+[624]$ configuration in other neighboring isotopes in Fig. 25. Similar values of the initial aligned angular momenta of these nuclei support the assigned configuration of this band.

Several high-$K$ bands have been observed in the nuclei in mass region $A \approx 180$ due to the presence of several high-
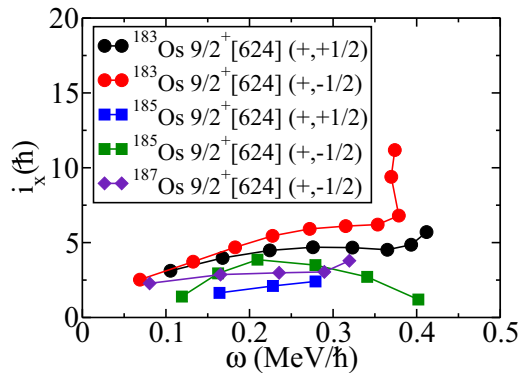


FIG. 25. Aligned angular momentum $i_x$ as a function of rotational frequency ($\omega$) for the band based on the $9/2^+[624]$ configuration in $^{183,185,187}$Os.
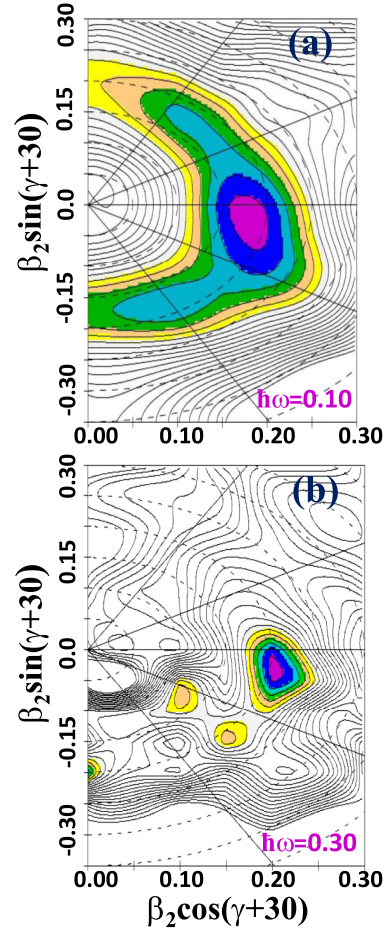


FIG. 26. TRS plots for the one-quasiparticle configuration of $\nu i_{13/2}$ corresponding to band 4 in $^{187}$Os for the rotational frequencies ($\hbar\omega$) 0.1 MeV (a) and 0.3 MeV (b). The contours are 250 keV apart.

$\Omega$ orbitals near the Fermi levels. Such high-$K$ bands have been reported in both even-even and odd-$A$ Os isotopes [4,22,25,56–58]. The high-$\Omega$ Nilsson orbitals $7/2^-[503]$, $11/2^+[615]$, and $9/2^+[624]$ lie near the neutron Fermi level of $^{187}$Os and the low-lying band structures based on these orbitals have been observed as well. These orbitals would contribute in generating high-$K$, multiquasiparticle states in $^{187}$Os. Band 7 in $^{187}$Os (see Fig. 2) with bandhead spin and parity of $25/2^+$ is possibly one such high-$K$ band based on the three-quasiparticle configuration of $\nu(h_{9/2})^2_{8^+} \otimes \nu 9/2^+[624]$. The plot of level energy vs spin for band 7 is also shown in Fig. 22. It clearly shows a different slope for band 7 compared to the other positive parity bands in $^{187}$Os. Smaller value of the inertia parameter, $A = 4.77$, corresponds to a larger moment of inertia for band 7. It suggests that this band is built on a multiquasiparticle configuration.

### 1. TRS calculations

The TRS calculation was performed corresponding to the configuration of band 4 and is shown in Fig. 26 for two

rotational frequencies, $\hbar\omega = 0.10$ and 0.30 MeV. A triaxial shape with $\beta_2 \approx 0.18$ and $\gamma \approx -35°$ has been obtained for the positive parity band 4. This estimated value of the triaxiality parameter $\gamma$ is in excellent agreement with that determined from the ratio of the excitation energies of the $15/2^+$ states in main and $\gamma$ bands. At the higher rotational frequency, a more rigid $\gamma$ deformation is predicted by the TRS calculations, which is again consistent with the experimental observation of $E_S(I)$ in Fig. 24.

It is worthwhile to point out that the TRS calculations give $\beta_4 = -0.021$ for $^{187}$Os on minimization. This is somewhat larger compared to the nominal value ($\approx 0.005$) estimated in other nuclei. Larger hexadecapole deformation ($\beta_4 \approx 0.05$) in the lighter osmium nuclei was reported long ago [59] with a possibility of hexadecapole vibration for the nuclei in this region [17]. More theoretical and experimental work is needed in future in order to verify whether the observation of a 564-keV $\gamma$ ray from the $19/2^+$ bandhead of band 6 to the $17/2^+$ state in band 4 is due to the consequence of the mixing of two different vibrational states.

## VI. SUMMARY

The excited states in $^{187}$Os have been studied by $\gamma$-ray spectroscopic technique. The reaction $^{186}$W($^4$He, $3n$) $^{187}$Os at 36 MeV of beam energy from the K-130 cyclotron at VECC, Kolkata was used to populate the states. The INGA spectrometer with seven Compton-suppressed clover HPGe detectors and one LEPS detector was used to detect the $\gamma$ rays. A new level scheme of $^{187}$Os, which is vastly expanded both horizontally and vertically, has been reported in this work with the placement of 94 new $\gamma$ rays. Evidence of triaxial shapes has been obtained for different configurations in this nucleus, appearing as long-axis rotation, large signature splitting, and $\gamma$ bands. The plot of double energy differences, $E_s(I)$, of the $\gamma$ band indicates a rigid triaxial deformation in $^{187}$Os in contrast

to the $\gamma$-unstable shape for the even-even core $^{186}$Os. TRS calculations support the triaxial nature of the bands in $^{187}$Os.

Band crossings, due to the alignment of a pair of particles, have been identified for the first time in all the bands in this nucleus and the band crossing frequencies indicate a moderate shell gap for $N = 110$ at a deformation of $\beta_2 \approx 0.2$.

The excellent degeneracy ($\Delta E_x$) and the one-unit difference in aligned angular momenta ($\Delta i_x$) values of the pseudospin Nilsson doublet bands 1 and 2 continues until the band crossing. This is one of the best examples of pseudopartner bands identified in nuclei. The deviation of these values at higher spins may be due to the onset of triaxiality in these bands, as predicted by the TRS calculations. Finally, the possibility of a high-$K$ band and hexadecapole vibration in $^{187}$Os has been pointed out. The results from the present work clearly suggest that the level scheme of $^{187}$Os is one of the few in which several nuclear structure aspects are manifested.

[1] I. Y. Lee, M. M. Aleonard, M. A. Deleplanque, Y. El-Masri, J. O. Newton, R. S. Simon, R. M. Diamond, and F. S. Stephens, Phys. Rev. Lett. **38**, 1454 (1977).

[2] G. Baldsiefen *et al.*, Nucl. Phys. A **574**, 521 (1994).

[3] T. Yamazaki *et al.*, Nucl. Phys. A **209**, 153 (1973).

[4] T. Shizuma, S. Mitarai, G. Sletten, R. A. Bark, N. L. Gjorup, H. J. Jensen, M. Piiparinen, J. Wrzesinski, and Y. R. Shimizu, Phys. Rev. C **69**, 024305 (2004).

[5] S. Nandi, G. Mukherjee, Q. B. Chen, S. Frauendorf, R. Banik, S. Bhattacharya, S. Dar, S. Bhattacharyya, C. Bhattacharya, S. Chatterjee, S. Das, S. Samanta, R. Raut, S. S. Ghugre, S. Rajbanshi, S. Ali, H. Pai, M. A. Asgar, S. DasGupta, P. Chowdhury, and A. Goswami, Phys. Rev. Lett. **125**, 132501 (2020).

[6] H. G. Börner, J. Jolie, S. J. Robinson, B. Krusche, R. Piepenbring, R. F. Casten, A. Aprahamian, and J. P. Draayer, Phys. Rev. Lett. **66**, 691 (1991).

[7] A. Guessous, N. Schulz, W. R. Phillips, I. Ahmad, M. Bentaleb, J. L. Durell, M. A. Jones, M. Leddy, E. Lubkiewicz, L. R. Morss, R. Piepenbring, A. G. Smith, W. Urban, and B. J. Varley, Phys. Rev. Lett. **75**, 2280 (1995).

[8] A. Guessous, N. Schulz, M. Bentaleb, E. Lubkiewicz, J. L. Durell, C. J. Pearson, W. R. Phillips, J. A. Shannon, W. Urban, B. J. Varley, I. Ahmad, C. J. Lister, L. R. Morss, K. L. Nash, C. W. Williams, and S. Khazrouni, Phys. Rev. C **53**, 1191 (1996).

[9] H. Hua, C. Y. Wu, D. Cline, A. B. Hayes, R. Teng, R. M. Clark, P. Fallon, A. Goergen, A. O. Macchiavelli, and K. Vetter, Phys. Rev. C **69**, 014317 (2004).

[10] L. M. Yang *et al.*, Chin. Phys. Lett. **18**, 24 (2001).

[11] R. Q. Xu *et al.*, Chin. Phys. Lett. **19**, 180 (2002).

[12] H. B. Ding *et al.*, Chin. Phys. Lett. **24**, 1517 (2007).

[13] X. L. Che *et al.*, Chin. Phys. Lett. **21**, 1904 (2004).

[14] X. L. Che *et al.*, Chin. Phys. Lett. **23**, 328 (2006).

[15] H. B. Ding, S. J. Zhu, J. H. Hamilton, A. V. Ramayya, J. K. Hwang, K. Li, YX. Luo, J. O. Rasmussen, I. Y. Lee, C. T. Goodin, X. L. Che, Y. J. Chen, and M. L. Li, Phys. Rev. C **74**, 054301 (2006).

[16] J.-G. Wang *et al.*, Phys. Lett. B **675**, 420 (2009).

[17] R. F. Casten, *Nuclear Structure From A Simple Perspective* (Oxford University Press, New York, 1990).

[18] A. S. Davydov and G. P. Filippov, Nucl. Phys. **8**, 237 (1958).

[19] J. Ndayishimye, E. A. Lawrie, O. Shirinda, J. L. Easton, J. J. Lawrie, S. M. Wyngaardt, R. A. Bark, T. D. Bucher, S. P. Bvumbi, T. R. S. Dinoko, P. Jones, N. Y. Kheswa, S. N. T. Majola, P. L. Masiteng, D. Negi, J. N. Orce, J. F. Sharpey-Schafer, and M. Wiedeking, Phys. Rev. C **100**, 014313 (2019).

[20] A. M. Bruce, C. Thwaites, W. Gelletly, D. D. Warner, S. Albers, M. Eschenauer, M. Schimmer, and P. von Brentano, Phys. Rev. C **56**, 1438 (1997).

[21] F. S. Stephens, M. A. Deleplanque, A. O. Macchiavelli, R. M. Diamond, P. Fallon, I. Y. Lee, and C. Schuck, Phys. Rev. C **57**, R1565(R) (1998).

[22] T. Shizuma *et al.*, Nucl. Phys. A **696**, 337 (2001).

[23] E. Ngijoi-Yogo, S. K. Tandel, G. Mukherjee, I. Shestakova, P. Chowdhury, C. Y. Wu, D. Cline, A. B. Hayes, R. Teng, R. M. Clark, P. Fallon, A. O. Macchiavelli, K. Vetter, F. G. Kondev, S. Langdown, P. M. Walker, C. Wheldon, and D. M. Cullen, Phys. Rev. C **75**, 034305 (2007).

[24] H. Sodan *et al.*, Nucl. Phys. A **237**, 333 (1975).

[25] C. Wheldon *et al.*, Nucl. Phys. A **652**, 103 (1999).

[26] The target was kept at an angle of about 55° with respect to the beam direction.

[27] S. Bhattacharya, *et al.*, Proc. DAE Symp. Nucl. Phys. **63**, 1156 (2018).

[28] S. Das *et al.*, Nucl. Instrum. Methods Phys. Res. A **893**, 138 (2018).

[29] D. C. Radford, Nucl. Instrum. Methods Phys. Res. A **361**, 297 (1995).

[30] R. K. Bhowmik, INGASORT manual (private communication).

[31] A. Krämer-Flecken *et al.*, Nucl. Instrum. Methods Phys. Res. A **275**, 333 (1989).

[32] S. Nandi, G. Mukherjee, T. Roy, R. Banik, A. Dhal, S. Bhattacharya, S. Bhattacharyya, C. Bhattacharya, M. A. Asgar, H. Pai, S. Rajbanshi, P. Roy, T. K. Ghosh, K. Banerjee, T. K. Rana, S. Kundu, S. Manna, R. Pandey, A. Sen, S. Pal, S. Mukhopadhyay, D. Pandit, D. Mandal, and S. R. Banerjee, Phys. Rev. C **99**, 054312 (2019).

[33] R. Palit *et al.*, PRAMANA J. Phys. **54**, 347 (2000).

[34] R. Banik, S. Bhattacharyya, S. Biswas, S. Bhattacharya, G. Mukherjee, S. Rajbanshi, S. Dar, S. Nandi, S. Ali, S. Chatterjee, S. Das, S. DasGupta, S. S. Ghugre, A. Goswami, A. Lemasson, D. Mondal, S. Mukhopadhyay, H. Pai, S. Pal, D. Pandit, R. Raut, P. Ray, M. Rejmund, and S. Samanta, Phys. Rev. C **101**, 044306 (2020).

[35] S. G. Malmskog, V. Berg, B. Fogelberg, and A. Backlin, Nucl. Phys. A **166**, 573 (1971).

[36] K. Ahlgren and P. J. Daly, Nucl. Phys. A **189**, 368 (1972).

[37] B. Harmatz, T. H. Handley, and J. W. Mihelich, Phys. Rev. **128**, 1186 (1962).

[38] M. S. Basunia, Nucl. Data Sheets **110**, 999 (2009).

[39] A. Arima, M. Harvey, and K. Shimizu, Phys. Lett. B **30**, 517 (1969).

[40] K. T. Hecht and A. Adler, Nucl. Phys. A **137**, 129 (1969).

[41] A. Bohr *et al.*, Phys. Scr. **26**, 267 (1982).

[42] R. D. Ratna Raju *et al.*, Nucl. Phys. A **202**, 433 (1973).

[43] C. Baktash *et al.*, Annu. Rev. Nucl. Part. Sci. **45**, 485 (1995).

[44] C. Wheldon *et al.*, Eur. Phys. J. A **19**, 319 (2004).

[45] T. D. Johnson and B. Singh Nucl. Data Sheets **142**, 1 (2017).

[46] D. E. Archer, M. A. Riley, T. B. Brown, D. J. Hartley, J. Döring, G. D. Johns, J. Pfohl, S. L. Tabor, J. Simpson, Y. Sun, and J. L. Egido, Phys. Rev. C **57**, 2924 (1998).

[47] T. Venkova *et al.*, Eur. Phys. J. A **18**, 1 (2003).

[48] G. Andersson *et al.*, Nucl. Phys. A **268**, 205 (1976).

[49] S. Saha, R. Palit, J. Sethi, S. Biswas, P. Singh, S. Nag, A. K. Singh, I. Ragnarsson, F. S. Babra, U. Garg, A. Goswami, E. Ideguchi, H. C. Jain, S. Kumar, M. S. R. Laskar, G. Mukherjee, Z. Naik, and C. S. Palshetkar, Phys. Rev. C **99**, 054301 (2019).

[50] E. Gueorguieva, C. Schück, A. Minkova, C. Vieu, F. Hannachi, M. Kaci, M. G. Porquet, R. Wyss, J. S. Dionisio, A. Korichi, and A. Lopez-Martens, Phys. Rev. C **68**, 054308 (2003).

[51] P. H. Regan *et al.*, Nucl. Phys. A **586**, 351 (1995).

[52] N. Perrin *et al.*, Z. Phys. A **359**, 373 (1997).

[53] W. Nazarewicz *et al.*, Nucl. Phys. A **435**, 397 (1985).

[54] W. Nazarewicz *et al.*, Nucl. Phys. A **512**, 61 (1990).

[55] G. Mukherjee *et al.*, Nucl. Phys. A **829**, 137 (2009).

[56] P. Chowdhury *et al.*, Nucl. Phys. A **485**, 136 (1988).

[57] D. M. Cullen *et al.*, Nucl. Phys. A **728**, 287 (2003).

[58] V. Modamio, A. Jungclaus, Z. Podolyak, Y. Shi, F. R. Xu, A. Algora, D. Bazzacco, D. Escrig, L. M. Fraile, S. Lenzi, N. Marginean, T. Martinez, D. R. Napoli, R. Schwengner, and C. A. Ur, Phys. Rev. C **79**, 024310 (2009).

[59] D. L. Balabanski and R. M. Lieder, Phys. Rev. C **49**, 2843 (1994).